Volume 20
Number 15
21 April 2024
Pages 3205–3378

# Soft Matter

rsc.li/soft-matter-journal

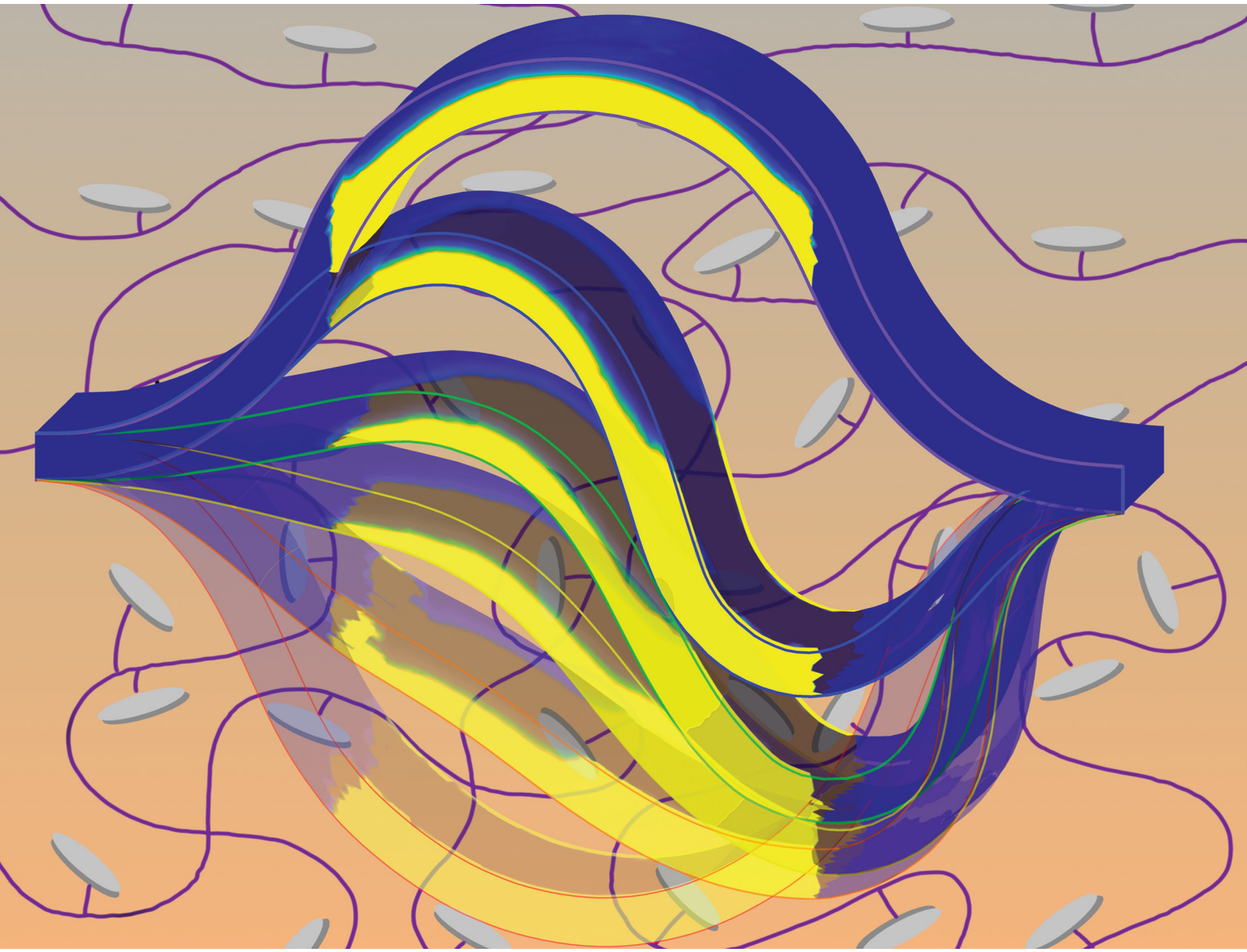

ISSN 1744-6848

ROYAL SOCIETY OF CHEMISTRY

**PAPER**
James T. Waters and Anna C. Balazs
Achieving controllable and reversible snap-through in pre-strained strips of liquid crystalline elastomers

Soft Matter

PAPER

View Article Online
View Journal | View Issue



Cite this: *Soft Matter*, 2024, **20**, 3256

# Achieving controllable and reversible snap-through in pre-strained strips of liquid crystalline elastomers†

James T. Waters and Anna C. Balazs *

Deformable, elastic materials that buckle in response to external stimuli can display "snap-through", which involves a transition between different, stable buckled states. Snap-through produces a quick release of stored potential energy, and thus can provide fast actuation for soft robots and other flexible devices. Liquid crystalline elastomers (LCEs) exposed to light undergo a phase transition and a concomitant mechanical deformation, allowing control of snap-through for rapid, large amplitude actuation. Using both a semi-analytical model and finite element simulations, we focus on a thin LCE strip that is clamped at both ends and buckles due to an initially imposed strain. We show that when this clamped, strained sample is exposed to light, it produces controllable snap-through behavior, which can be regulated by varying the light intensity and the area of the sample targeted by light. In particular, this snap-through can be triggered in different directions, allowing the system to be reset and triggered multiple times. Removing the light source will cause the system to settle into one of two stable states, enabling the encoding and storage of information in the system. We also highlight a specific case where removing the light source removes the induced buckling and returns the material to an initially flat state. In this case, the system can be reset and form a new shape, allowing it to function as a rewriteable haptic interface.

Received 10th January 2024,
Accepted 18th March 2024

DOI: 10.1039/d4sm00037d

rsc.li/soft-matter-journal



## I. Introduction

Soft elastic materials that undergo a reversible buckling can display "snap-through", which involves a transition between stable buckled states. The occurrence of snap-through is highly desirable for a range of applications since this mechanism can magnify the response of the system to external stimuli and prompt the rapid release of stored potential energy. The latter attributes are beneficial for fast actuation in devices[1] and soft robots.[2,3] Liquid crystalline elastomers (LCEs) can display snap-through when exposed to an external source of heat or light, as experimentally demonstrated in the thermal actuation of curved LCE surfaces,[4] and pre-strained thin LCE strips under low illumination.[5,6] In LCEs containing nematically aligned mesogens, the imposed heat or light triggers a transition from the ordered nematic (N) to disordered isotropic (I) state. This N–I transition has a pronounced effect on LCE micro-pillars anchored to a surface where increasing the light intensity can generate a traveling wave of N–I transitions, which can propagate through the entire width of the sample, and thus produce a time-dependent variation in the relative size of the nematic and isotropic regions.[7] Concurrently, the wave of N–I transitions triggers a wave of mechanical deformation. When the entire face of the LCE post is illuminated, this propagating opto-mechanical response drives the whole post to dynamically bend, turn, twist and display "dance-like" movements.[8,9] For practical applications, however, it could be useful to localize the light-induced deformations and thus form, for example, bendable joints or hinges between stiff sections, analogous to the control over buckling afforded by pneumatic vasculatures[10] in other materials. Using a combination of modeling approaches, we vary the width of the aperture controlling the amount of light that hits the surface of a clamped sample. In this way, we localize the N–I phase transition to certain regions and attain spatiotemporal control over the buckling in the material. Furthermore, we find a specific range of aperture sizes that actuate the desired snap-through and thus are ideal candidates for soft actuators.

We initially focus on a free (unclamped) LCE strip, in the absence of light to obtain a frame of reference for the more complex scenarios considered here. (In the case of the free strip, the strip's center of mass is fixed, but there is no constraint on the free ends, other than remaining in the $x$–$y$

*University of Pittsburgh, Department of Chemical and Petroleum Engineering, USA. E-mail: balazs@pitt.edu*

† Electronic supplementary information (ESI) available. See DOI: https://doi.org/10.1039/d4sm00037d

plane). We then systematically analyze the behavior of this free strip in the presence of light and similarly, determine the behavior of the clamped strip with and without illumination. As discussed below, these studies reveal that illuminating a clamped sample induces a curvature that varies non-monotonically with the light intensity. Additionally, we find that the illuminated, buckled strip will encompass both positively and negatively curved regions along its length, leading to a non-trivial dependence of the snap-through behavior on characteristics of the light. Moreover, we find that the specific buckling response can be controlled by tailoring the interaction between a curvature induced by the initial strain (compression) and a curvature induced by the light.

The presence of both positive and negative curvature noted above proves to be of particular benefit for technological applications. Targeting these specific regions with light permits a contact-free reversal of the snap-through, enabling the strip to buckle in either an upward or downward direction. Buckling in this upward or downward state remains stable when the light is removed. Viewing the up or down state as a separate bit (*e.g.* as a one or a zero) the system can be used to record and store information *via* the buckled state. The message can be rewritten with the new application of light. This setting and resetting capability is a necessary step in using snap-through in elastic systems for digital logic.[11]

Programming arbitrary director fields into LCEs can be accomplished *via* a magnetic field during cross-linking.[12] The induced alignment enables not only the snap-through of LCE's under an initial strain, but also the introduction of strain and buckling to initially flat structures. The reversibility and control of such a system would have clear applications for a haptic interface device.[13,14]

# II. Methods

To avoid confusion, in the subsequent discussion, we use the word ''strip'' to refer to the material and the word ''beam'' to refer to the light. Our analysis of this system proceeds on two tracks. The first is a finite element model we have previously used to explore liquid crystalline elastomer systems,[9] and which we have validated against experimental results.[8,12] This model can be used to predict the response of LCE films to light or changes in temperature as a function of the light intensity and position, as well as the features of the LCE device such as thickness, length, and director orientation. Additionally, this model can be used to establish the general effect of these parameters on length, thickness, and curvature changes, which can be used to inform a semi-analytical model that can predict the buckled shapes of the elastomer, more quickly exploring the parameter space than the finite element simulations alone.

## A. Finite element simulations

Our finite element method describes the interaction of bulk and shear deformations in terms of a free energy using the Gent hyperelastic model, along with a strain–nematic coupling. The elastic terms are given as

$$F_{\text{elastic}} = -\frac{\mu J_{\text{m}}}{2}\ln\left(\frac{J_{\text{m}} - I_1}{J_{\text{m}} - 3}\right) + \frac{\kappa \ln^2 J}{2} \tag{1}$$

where the quantities $I_1$ and $J = \sqrt{I_3}$ come from the first and third invariants of the strain tensor, respectively. $\mu$ is the shear modulus and $\kappa$ is the bulk modulus, while $J_{\text{m}}$ is a constant describing the maximum extension of the constituent polymer chains, here set to 30. Viscoelastic effects are accounted for with a Kelvin–Voigt model,[15] which gives a dissipation function in terms of the velocity gradient tensor computed from the finite element mesh.

The strain–nematic coupling is an additional free energy term that connects the deformation gradient tensor in the material frame to the orientation of the nematic director that is hard-coded into the material. This coupling is proportional to the change in order parameter, causing the material to contract along the axis of the nematic director and expand along the orthogonal axis when it transitions from a nematic state to a less ordered isotropic state ($\alpha\Delta S < 0$).

$$F_{\text{nem}} = \alpha\Delta S\epsilon_{ij}\left(n_i n_j - \frac{1}{3}\delta_{ij}\right), \tag{2}$$

where $n$ is a unit vector defining the nematic director, fixed in the material frame, and $\alpha$ is a constant describing the strain–nematic coupling, set to $\alpha\Delta S/\mu = 0.18$ to match experimentally observed deformations.[12] Intrinsic curvature can be introduced into this system in different ways. When the phase transition is induced by UV light, the change in order parameter can be localized to one side of the LCE strip. This will result in an order parameter that varies through the thickness of the strip, meaning one face of the strip will expand or contract more than the other. The order parameter is expected to fall off exponentially with depth at low intensities, following the decay of light intensity according to Beer's law. However, at higher intensities, the system will be described by a feedback loop where the light-induced isomerization reduces the opacity of the material, allowing more light to penetrate deeper into the elastomer.[7] The isomerization is described by a differential equation in time

$$\frac{\mathrm{d}n_t}{\mathrm{d}t} = -\Gamma \ln_t + \frac{1 - n_t}{\tau}, \tag{3}$$

where $n_t$ is the ground-state *trans* fraction, $I$ is the light intensity, $\Gamma$ is the isomerization rate, and $\tau$ is the relaxation rate. While the attenuation in light intensity as a function of depth is governed by the fraction of *trans* isomers

$$\frac{\mathrm{d}I}{\mathrm{d}x} = \frac{I}{\gamma\Gamma n_t} \tag{4}$$

At late times and high intensities, this approaches a logistic function with respect to depth.

The coordinates of the finite element mesh are updated in time using a leapfrog integration method, with accelerations derived from the gradient of the free energy with respect to the mesh coordinates. Alternating between each of these mesh

updates, the isomerization at each node is also updated. This is done by calculating the light path through the material to each point, using the current mesh coordinates, and applying an attenuation based on the opacity stored for each element at that point in time to obtain the intensity at the mesh points.

### B. Semi-analytical model

The space of possible parameters for finite element simulations can be more quickly covered if we develop a semi-analytical model that attempts to capture the bending energy of elastic strips under compression. This will pare away the precise details of deformation of the liquid crystalline elastomer and give us a simplified view, which we can use to quickly predict the behavior of the bending strip throughout a multivariable parameter space.

Here, we describe the shape of the strip in terms of a deflection angle $\theta$ away from the $x$-axis, as a function of the longitudinal coordinate $\alpha$ in the material frame. Here we have normalized this coordinate to run from 0 to 1 over the length of the strip. This will make it simpler to describe the bending energy as a function of the change in this coordinate, the trade-off being that it becomes more complicated to impose boundary constraints that are measured in Cartesian laboratory frame coordinates. The energy is assumed to be quadratic in terms of the change in deflection, and scaled by a bending moment that can vary along the length of the strip.

$$U(\alpha) = \frac{1}{2}\frac{Mh^2}{l}\dot{\theta}^2 \tag{5}$$

where $h$ is the strip thickness, $l$ is the lab-frame length as a function of the longitudinal position, and $M$ is an elastic modulus. This is corresponds to the bending energy of a deformed rod found in texts on elasticity.[16] The end-to-end displacement can be found by integrating with respect to the material frame coordinate, to obtain

$$\Delta_x = \int_0^1 l\cos\theta(\alpha)\mathrm{d}\alpha \tag{6a}$$

$$\Delta_y = \int_0^1 l\sin\theta(\alpha)\mathrm{d}\alpha \tag{6b}$$

These displacements are what is held constant when the strip is clamped or pinned at the ends. We can enforce these constraints by writing down a Lagrangian for the system with two undetermined multipliers.

$$L = \frac{1}{2}\frac{Mh^2}{l}\dot{\theta}^2 - \lambda_x l\cos\theta - \lambda_y l\sin\theta \tag{7}$$

This can then give an equation of motion for the function $\theta$

$$\frac{Mh^2}{l^2}\ddot{\theta} - \lambda_x\theta - \lambda_y = 0 \tag{8}$$

where we have approximated the trigonometric functions by the leading order of their Taylor expansions. This is satisfied by a general sinusoidal solution

$$\theta(\alpha) = A\sin(\omega\alpha + \phi) + C \tag{9}$$

The amplitude and wavelength of this solution can be determined from the boundary conditions. In the case of clamped boundary conditions, the orientation of the strip will be fixed and $\theta$ will take on a prescribed value at the ends. In the case of pinned boundary conditions, we instead have the derivative $\theta$ approaching zero at the ends.

For a strip that has a piecewise constant thickness, we can apply the solution in eqn (9) to the different regions; the undetermined multipliers will be constant between the regions, allowing us to determine the ratio of the wavelengths.

$$\theta_L(\alpha) = A_L\sin(\omega_L\alpha + \phi_L) + C \tag{10a}$$

$$\theta_R(\alpha) = A_R\sin(\omega_R\alpha + \phi_R) + C \tag{10b}$$

where

$$\frac{\omega_L{}^2 h_L{}^2}{l_L{}^2} = \frac{\omega_R{}^2 h_R{}^2}{l_R{}^2} \tag{11}$$

We also require continuity of the deflection angle $\theta$, and a condition on the derivative of the deflection angle

$$\frac{h_L{}^2\dot{\theta}_L}{l_L{}^2} = \frac{h_R{}^2\dot{\theta}_R}{l_R{}^2} \tag{12}$$

to satisfy the equations of motion from the Lagrangian. Physically, we see that this corresponds to balancing the moments across the boundary. Together, these are enough information to find a solution for the deflection angle along the whole length of the strip, with each segment of the piecewise solution introducing three new parameters but with three boundary conditions relating it to the solution in the neighboring region. This method will fact produce several solutions, corresponding to buckled shapes of different wavelengths. The lowest wavelength of these, with the smallest bending energy, is chosen for comparison with the finite element results. The system is also invariant under sign changes to the amplitude $A$ when the deflection angle is clamped at zero at the ends, corresponding to the equal energy of up and down buckled states.

The partial isomerization and variation in the nematic director can both introduce an intrinsic curvature to the strip that will be evident in the absence of any constraints at the end. This curvature will manifest in the Lagrangian as a constant offset for the quadratic bending energy

$$L = \frac{1}{2}\frac{Mh^2}{l}\left(\dot{\theta} - \kappa\right)^2 - \lambda_x l\cos\theta - \lambda_y l\sin\theta \tag{13}$$

The resulting differential equation will be satisfied by the same general sinusoidal function as before. If the intrinsic curvature varies between regions of the strip, the matching condition between the two regions is now

$$\frac{h_L{}^2\left(\dot{\theta}_L - \kappa_L\right)}{l_L{}^2} = \frac{h_R{}^2\left(\dot{\theta}_R - \kappa_R\right)}{l_R{}^2} \tag{14}$$

Additionally, the constant in the Lagrangian breaks the symmetry between the two solutions. Now we have not only a family of solutions at different wavelengths but also distinct shapes for the upward and downward buckled solutions. While the

 

Lagrangian ensures that both solutions will be stationary solutions of the equations of motion, these may represent a local minimum or a saddle point in the space of possible contour shapes. Additional analysis can assess the stability of these states, determining which conformation the buckled strip will actually adopt.

The stability of these states can be predicted through a discretization of the system into one-dimensional elements and computing the Hessian matrix from the second derivatives, as discussed in ref. 6. While the bending moment and induced curvature can vary stepwise between the illuminated and non-illuminated regions in the continuous model, we find it is necessary to introduce an interpolated, and therefore differentiable, value of the curvature and bending moment for elements crossing the light boundary. Without considering this contribution to the change in free energy with respect to position, the system cannot correctly predict the occurrence of snap-through behavior.

# III. Results

As detailed below, light gives rise to a propagating isomerization front as it passes through the material and produces a gradient in the local nematic ordering in the sample. The latter gradient exerts a strain that induces curvature in the strip. If the strip is clamped at both ends, the system will manifest additional curvature due to the buckling arising from the strain at the fixed ends. Varying the balance between these two sources of bending produces a range of the unusual non-monotonic behavior described in the following sections.

## A. Behavior of unclamped LCE strip

Focusing on a free (unclamped) elastic LCE strip, we determine the effect that varying the intensity of the applied light has on other variables, such as length, thickness, and induced curvature that dictate the buckled shape of the strip (Fig. 1A–D). In the systems considered here, the LCE contains photo-responsive azobenzenes; the material undergoes isomerization as the applied light excites the *trans* isomers in the azobenzenes into the *cis* state. The degree of isomerization determines the opacity of the material (*i.e.*, the penetration depth); Fig. 1A shows how the degree of isomerization falls off as a function of depth in a free segment of an LCE strip for different light intensities at late times. The degree of isomerization also dictates the change in the nematic order parameter, $\Delta S$, within the material. Here, $\Delta S$ to assumed to be proportional[17] to the fraction of the azobenzenes in the excited, *cis* state, $n_c = (1 - n_t)$, where $n_t$ is the fraction in the *trans* state.

For a nematic director uniformly oriented along the long axis of the LCE, an illuminated strip will contract along this axis and expand along the orthogonal axes, and thus, the sample becomes shorter and thicker; Fig. 1C shows how the length of the material decreases and the thickness increases as a function of light intensity. (In these simulations, we constrained the expansion of the material along the third axis, out of the plane of the page in the figure.) At high intensity, the thickness approaches 1.33× its initial value, while the length contracts to 0.75× its original value. The bulk modulus of the material is assumed to be significantly larger than the shear modulus of the material, ($K$ = 28 MPa, $\mu$ = 570 kPa, eqn (1)), maintaining the volume within 1% of its value in the initial, unstressed state. These values and the strain–nematic coupling in eqn (2) correspond to experimentally measured parameters for LCE materials.[8,12]

When the change in order parameter varies through the thickness of the material, the system exhibits an induced curvature, as depicted in Fig. 1B, where the color bar indicates the degree of isomerization (which is proportional to the change in nematic order parameter) from 0 (blue) to 1 (yellow). The exposed face contracts while the non-illuminated face retains its original length and the ends of the strip bend towards the light. Fig. 1D shows how the magnitude of this curvature varies with light intensity. At low intensity, the order parameter varies only slightly across the material and so the deformation is small (Fig. 1B(i)). At high intensity, the change in the order parameter is large, but approaches a constant value through the material, causing it to contract but not bend (Fig. 1B(iii)). The curvature is greatest at intermediate intensities (Fig. 1B(ii)), where isomerization is significant on one side of the strip and less on the other side. The maximum value of the bending achieved for this thickness is $6.4 \times 10^{-3}$ rad $\mu m^{-1}$ at an intensity of 40 mW $cm^{-2}$.

## B. Behavior of clamped, pre-strained LCE strip and appearance of snap-through

**1. In absence of light.** If the nematic director is oriented along the long axis of the strip (as in Fig. 1) and the strip is clamped at both ends, then an initial applied compression drives the strip to buckle, similar to the geometry explored by Shankar *et al.*[5] Without light, the system remains symmetric in the longitudinal direction; the strip can buckle upward or downward with equal probability. Without light to induce a phase change, the deflection angle along the buckled strip will follow a sinusoidal function (Fig. 3A); this deflection corresponds to the slope of the strip along its length. The bending energy of the strip is proportional to the derivative squared of this function, as in eqn (13). For clamped boundary conditions, this deflection angle is held fixed at zero at both ends; hence, it must cover a full wavelength to satisfy the boundary conditions. (Fig. 3A). Consequently, both the upward buckled (blue curve) and downward buckled (red curve) will exhibit regions of positive and negative curvature, as seen from the slope of the deflection angle, which characterizes the curvature. The two states will have the same bending energy; the difference will be that the negatively curved region is in the middle for the upward-buckled state but at the edges for the downward-buckled state.

**2. In presence of light.** The symmetry of the system is broken when the strip is subjected to light from one direction (directed upwards along the vertical axis for all of the following cases). In this geometry, a nematic–isotropic transition induced

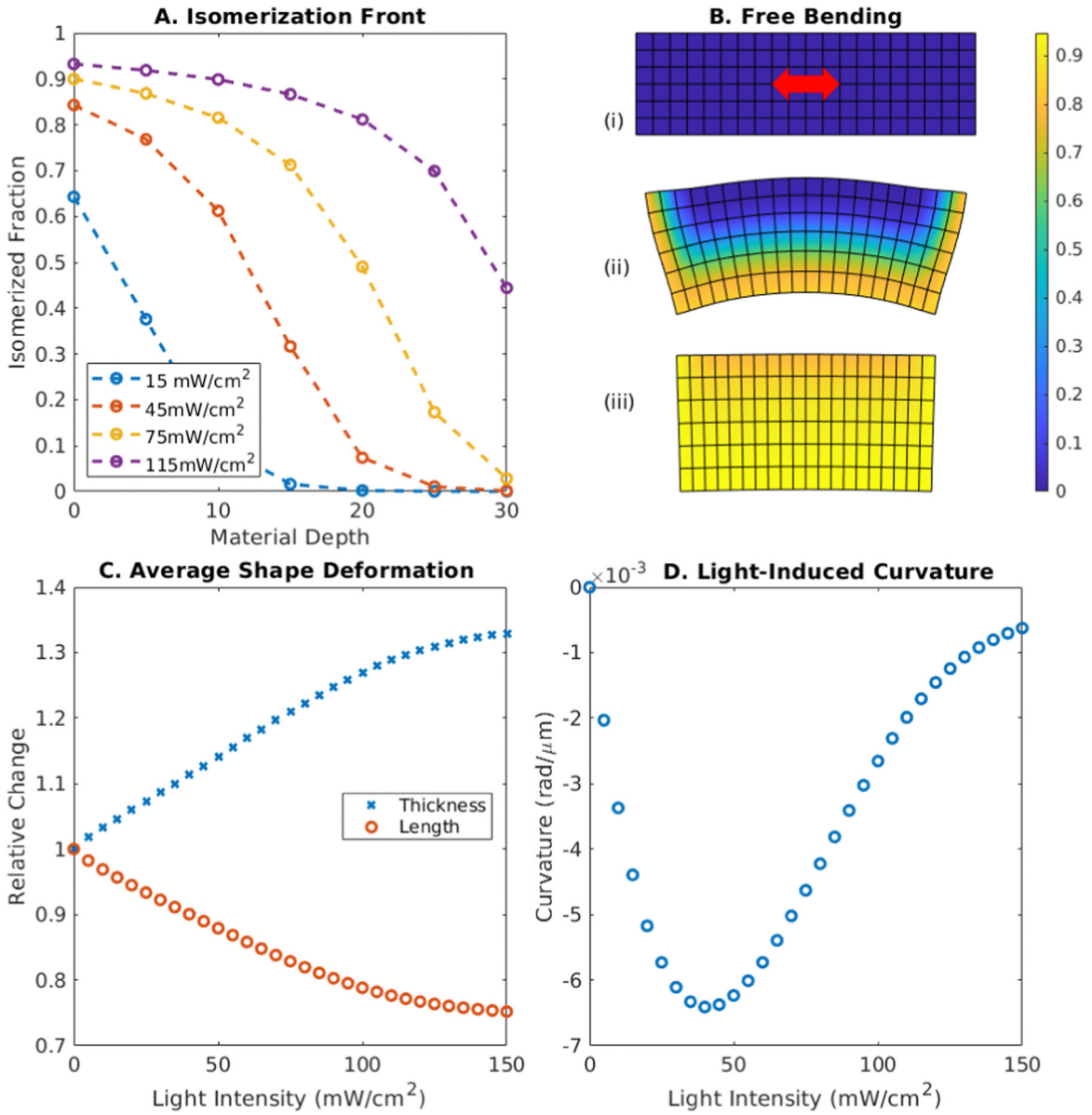


Fig. 1 Free LCE response as a function of light intensity. (A) Fraction of excited *cis* isomers as a function of material depth at different light intensities. (B) Resulting conformations for (i) zero intensity, (ii) intermediate intensity (45 mW $cm^{-2}$) and (iii) high intensity (150 mW $cm^{-2}$), from top to bottom. Colors indicate the degree of isomerization from 0 (blue) to 1 (yellow). Isomerization causes the strip to contract along the long axis and become thicker. At intermediate intensity, the variation in isomerization through the thickness causes bending towards the light. At high intensity, the contraction approaches a constant value and this bending relaxes. (C) Average length and height change through the thickness of the material *versus* intensity. Under high intensity light, the material contracts to 0.75× its initial length and expands to 1.33× its initial thickness. (D) Curvature along length of material as a function of intensity, reflecting the behavior in (B). The maximum amplitude for the bending achieved is 6.4 × $10^{-3}$ rad $\mu m^{-1}$ at an intensity of 40 mW $cm^{-2}$.

by light (or heat) will lead to a shortening of the strip, relieving some of the stress applied at the boundaries. From the free strip behavior shown in Fig. 1, we anticipate two effects due to the incident light. First, the light-induced curvature at intermediate intensities will create an energy difference between the two buckled states (whether this light induced curvature has the same or opposite sign as the initial, strain induced curvature). Second, the light-induced contraction of the strip relieves some of the initial strain and lowers the barrier between the two buckled states. As noted in the Introduction, if the applied light now passes through an aperture that restricts the size of the illuminated region, we hypothesize that the resulting localized opto-chemo-mechanical effects will lead to new dynamic behavior.

To probe this behavior, we fix the light intensity at 45 mW $cm^{-2}$ and examine the system's response at two different aperture widths. The values of the other parameters are fixed as follows: the initial strain of $(L_0 - L)/L_0 = 0.3$; strip thickness

 

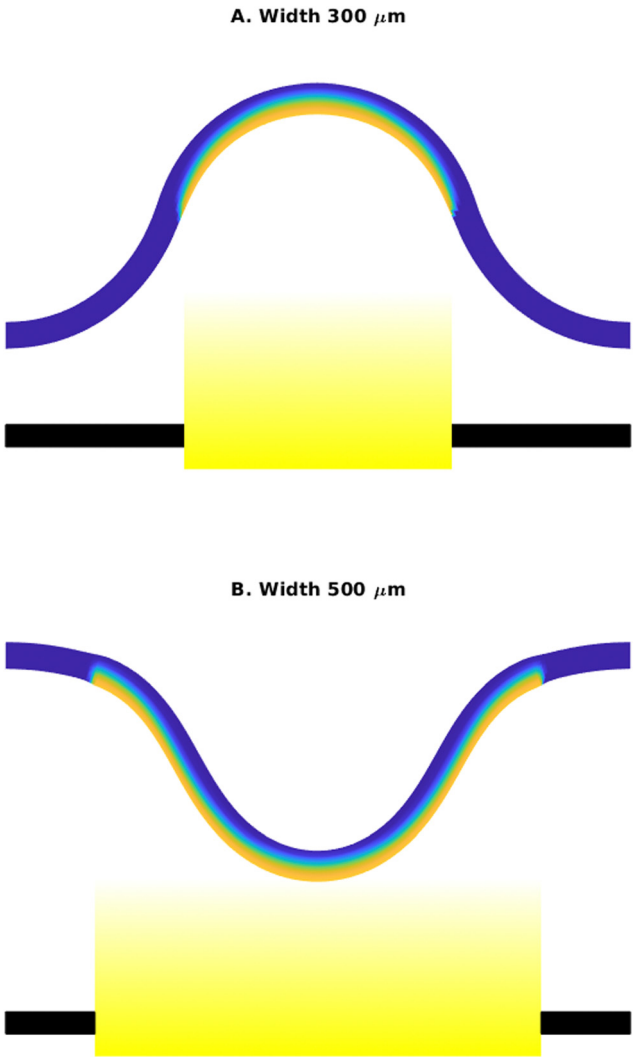


Fig. 2 Final shapes from finite element simulations, beginning from the downward buckled state. (A) Aperture width 300 μm and intensity 45 mW cm$^{-2}$. Beginning from a state buckled towards the light source, the contraction and curvature induced by exposing the middle of the LCE strip to light cause the strip to snap through to a state buckled away from the light. (B) Aperture width 500 μm and intensity 45 mW cm$^{-2}$. When a larger region of the LCE strip is exposed to light, it fails to initiate snap-through.

30 μm; and relaxed length 1 mm. Fig. 2 shows the shapes of the buckled strip that were obtained with the finite element simulations for a light intensity 45 mW cm$^{-2}$ and aperture widths of 0.3 mm (Fig. 2A) and 0.5 mm (Fig. 2B). In both cases, the strip was initially buckled downward, towards the light source. The initial configuration was obtained by applying the initial strain and allowing the system to relax in the nematic state, without any phase change (*i.e.*, no light). The colors reveal the degree of isomerization, as indicated by the color bar in Fig. 1B, where blue corresponds to the unexcited *trans* state and yellow to the excited *cis* state. For this intensity, the exposed face of the strip undergoes a nematic–isotropic transition, while the side of the strip not exposed to the light remains non-isomerized. For an aperture width of 0.3 mm (30% of the relaxed length) the strip, initially buckled towards the light, then exhibits a snap-through away from the light. For a wider aperture (0.5 mm), however, the elastomer remains buckled towards the light (Fig. 2B).

The semi-analytical model indicates that in the presence of a light source, buckling away from the light is energetically favorable for all cases, as seen in Fig. 3B and C. Fig. 3B displays the energy of the up and down states predicted from the semi-analytical model as function of light intensity for an aperture width of 400 μm, marked with open triangles. At low intensities, both states have some buckling energy associated with the initial imposed strain. As the intensity and light-induced curvature increases, the energy of the upward-buckled state decreases because the light-induced curvature (arising from the phase change on the illuminated face of the strip) and curvature due to the initial compressive strain have the same sign at the center of the strip. Thus, both the applied light and strain favor the same direction of buckling. The energy of the downward-buckled state, however, increases because the light induced curvature (see Fig. 2B) is opposite in sign to the initial strain-induced curvature. At high intensities, the difference between the two states decreases again as the light-induced curvature (Fig. 1D) decreases in magnitude. This difference between states is accompanied by a corresponding energy released during snap-through. By computing the free energy in the finite element mesh from eqn (1) and (2) before and after snap-through, we estimate this release to be approximately 3 mJ cm$^{-3}$ across a range of intensities (ESI,† Fig. S1).

We now fix the light intensity at 60 mW cm$^{-2}$ and vary the aperture width to obtain the plot in Fig. 3C, which shows the predicted energy of the two states as a function of the illuminated fraction at a fixed intensity. For the upward buckled state, the light-induced curvature in the middle of the strip works cooperatively with the curvature from the initial strain, reducing the free energy. When the illuminated area expands further from the center, the strain-imposed curvature changes in sign, as can be seen by comparing the bending near the clamped ends in Fig. 2A and B. Consequently, the bending energy for the upward state increases, as shown by the blue triangles in Fig. 3C near an illuminated fraction of 0.5.

For the downward buckled state, however, the trend is reversed, where the light-induced curvature (Fig. 2B) works against the strain-imposed curvature at the center, but cooperatively towards the edges. As more of the strip is illuminated, the difference between the two states decreases and they converge on a higher energy than the unilluminated strip. While some energy is relieved by the average contraction, more is introduced by the light induced curvature at this intensity.

### C. Phase diagram for system and stability of the different buckled states

Despite the fact that the upward buckled state has a lower free energy across all parameters, if the strip is initially buckled towards the light, then the system can become trapped in a non-equilibrated state that has a higher free energy than the upward buckled state for a specific range of intensities and aperture widths. Using the same initial conditions with the

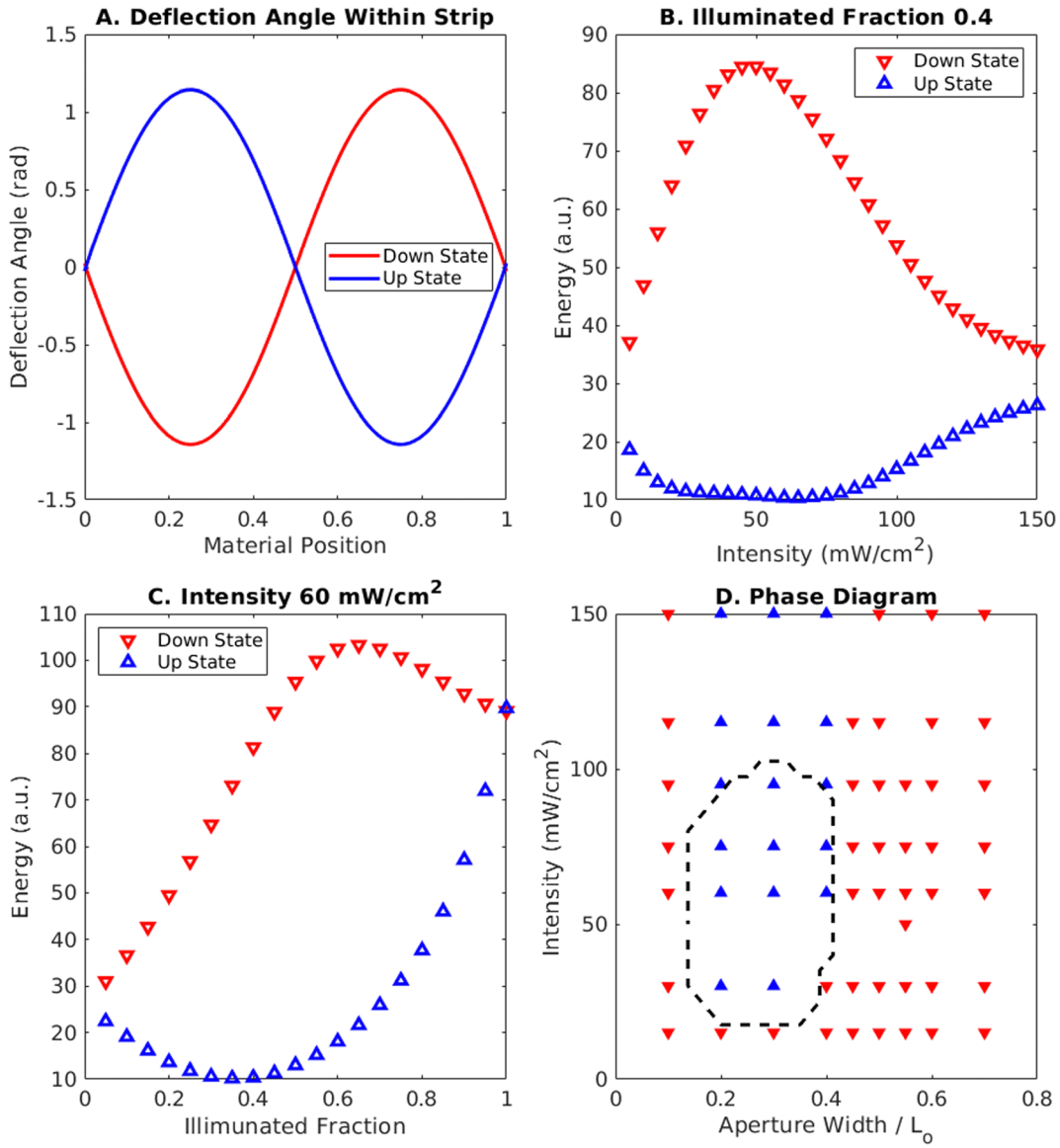


Fig. 3 Free energy and phase diagram. (A) Deflection angle along clamped, buckled strip for downward (red) and upward (blue) buckled state. For clamped boundary conditions, the deflection follows a sine wave through a full period. Bending energy along the strip is proportional to the derivative squared of the deflection angle. (B) Free energy for downward and upward buckled state as a function of light intensity for an illuminated width 400 μm. The induced curvature reduces the energy in the upward-buckled state, where the sign of the induced curvature matches the sign of the curvature imposed by the initial strain at the center. For the downward buckled beam, these signs differ and the bending energy increases. At high intensities, the light-induced curvature decreases and the free energy difference between the two states is reduced. (C) Free energy for downward and upward buckled state as a function of illuminated width for a fixed intensity 60 mW cm$^{-2}$. When the middle of the strip is illuminated, the light-induced curvature and the strain-imposed curvature have the same sign for the upward-buckled case (blue triangles), reducing energy, and opposite signs for the downward-buckled case (red triangles), increasing energy. At larger aperture widths, the signs of light-induced curvature and strain-imposed curvature no longer match across the whole aperture width and the bending energy increases for the upward-buckled case. The reverse trend occurs for the downward-buckled case, and the two energies converge when the entire strip is illuminated. (D) Phase diagram for snap-through as a function of aperture width and intensity. Filled blue triangles indicate parameters for which snap-through occurred in finite element simulations, while filled red triangles indicate parameters for which the system is trapped in the initial state. The black dashed line encloses the region where snap-through occurs predicted by the semi-analytical model. This agrees with the finite element results, except for high intensities where the semi-analytical model predicts stability in the downward-buckled state at all aperture widths, but snap-through occurs for the finite element simulations as the system passes through an unstable state as the isomerization front propagates through the material.

strip buckled downwards, we constructed a phase diagram mapping the final state as a function of the light intensity and aperture width in Fig. 3D. The data from the finite element simulations are marked by the filled triangles: red, filled downward pointing triangles represent finite element simulations where the strip remained buckled towards the light (downwards), whereas the blue filled upward triangles correspond to cases where snap-through occurred.

 

The black dashed line encloses the region where the upward buckled state is stable, as predicted by the semi-analytical model. Note the good agreement between this region and the snap-through region observed in the finite element simulations (marked by filled triangles). This unstable region forms an island that is bounded above and below for values of both aperture width and light intensity parameters. The plot indicates the light intensity and aperture width must be neither too low nor too high to induce instability in the structure.

**1. Dependence of snap-through on aperture width at fixed intensity.** In Fig. 4, the final shape of the strip obtained from the finite element simulation is plotted in grey, alongside the shapes from the semi-analytical model for up (in blue) and down states (in red). Fig. 4A–C show the systems' behavior for different aperture widths at a fixed light intensity of 60 mW $cm^{-2}$. The curves predicted from the semi-analytical model are dimensionless and are scaled by the relaxed length of the strip in the finite element simulation for the purpose of comparison in this figure. Fig. 4D–F show the deflection angle representation of the corresponding system.

The behavior in Fig. 4A can be understood by looking at the deflection angle along the length of the elastomer in Fig. 4D. For the clamped boundary conditions, this angle follows a sine function through a full period, encompassing areas of both positive and negative curvature. The curvature is defined by the derivative of this deflection angle along the length of the material. For the upward buckled state (drawn in blue), the negatively curved region lies in the middle of the simulated strip. Conversely, for the downward buckled state (in red), the negatively curved region lies at the edges.

The plot in Fig. 4D indicates that when a small region in the middle of the strip is illuminated, the downward curvature induced by the light causes a jump in the derivative of the deflection angle, along with an increased wavelength caused by the increased bending moment. This behavior makes the boundaries of the illuminated region identifiable by cusps in

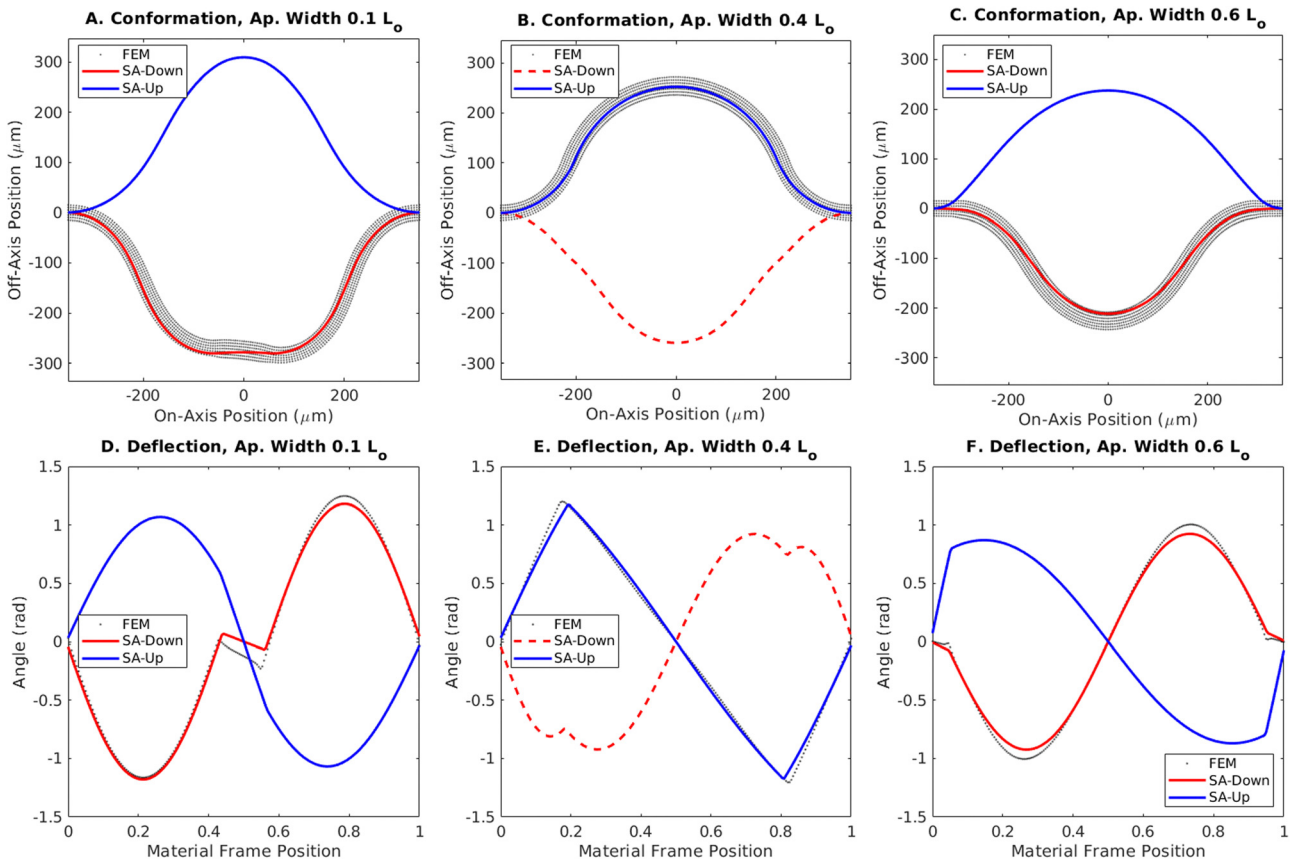


Fig. 4 Dependence of snap-through on aperture width at fixed intensity 60 mW $cm^{-2}$. Red and blue curves show the predicted shapes of the upward and downward buckled states, respectively, while black dotted shapes are the final conformations from finite element simulation. (A) For a narrow aperture width (100 μm), the curvature induced in a small region in the middle of the strip fails to induce snap-through (B) For a wider aperture (400 μm), the downward buckled state becomes unstable (dashed line) and the strip snaps through to the upward state. (C) For an even wider aperture (600 μm), the system is stable in the downward state, as it was for the narrow aperture. (D) Deflection angle for simulation in (A) alongside predictions from semi-analytical model. A sharp kink is visible in the illuminated region (black and red curves) but the system remains stable. (E) Deflection angle for simulation in (B). The induced curvature makes snapping through to the upward-buckled state favorable. (F) Deflection angle for simulation in (C). The region of light-induced curvature encompasses both positively and negatively curved regions, and the energy difference between states is not enough to overcome the barrier between them.

the angle distribution, separating the regions with and without light-induced curvature. This change, however, is not sufficient to reduce the potential energy barrier between states and the simulated strip remains in the downward buckled state, near the semi-analytical prediction for these parameters.

As the area of incident light is increased to 400 μm (centered over the middle of the strip) (Fig. 4B and E), the energy difference between the two states grows larger (Fig. 3C) and the downward buckled state becomes unstable (red line, dashed to indicate instability). The system involving this larger aperture displays essentially the same change in the bending moment and induced curvature as in the narrow aperture case, but here the induced curvature at the edges of the strip (see Fig. 2) promotes the snap through from the downward state. Additionally, the difference in wavelength between the illuminated and unilluminated regions is most readily apparent here in the unstable downward buckled case, where the quarter wavelength in the unilluminated region can be seen in the separation from the edge to the local minimum on one side of the cusp, giving a wavelength $0.56L$, where $L$ is the relaxed length of the strip. On the other hand, the half wavelength in the thicker illuminated region can be found from the separation of the minimum and maximum points between the cusps, exhibiting a wavelength of $0.90L$. The same ratio of wavelengths, computed to be 0.62, will exist across different aperture widths and for both upward and downward buckled states for this illumination; however, it will be difficult to discern when either the illuminated or unilluminated region is too small to exhibit a local extremum.

At even larger illumination widths (600 μm in Fig. 4C and F), the light covers more than half a period of the deflection angle, meaning it covers regions of both positive and negative curvature in either the upward or downward buckled case. Here, the induced curvature at the edges of the strip works against the snap-through from the downward state, rather than promoting it (as in Fig. 4B), and the downward buckled state is once again stable, as in the narrow aperture case in Fig. 4A. The reoccurrence of bistability correlates with the decrease in energy between the two states predicted as the illuminated width encompasses the entire strip in the semi-analytical model as seen at the right of Fig. 3C.

**2. Dependence of snap-through on light intensity at fixed aperture width.** Fig. 5 shows the final state at various light intensities at a fixed aperture width of 300 μm for both the finite element simulations (in grey), and the semi-analytical model. Dependence on intensity can be understood as follows: as the light intensity increases, the gradient in the degree of isomerization creates a curvature large enough to overcome the barrier between the states. At very high intensities, however, the change in phase is uniform through the strip as seen in Fig. 1, and the light induced curvature is no longer present; hence, the barrier between the states reappears.

At low intensity (15 mW $cm^{-2}$) in Fig. 5A and D, the light does not induce enough curvature or relieve enough strain to overcome the energy barrier and the finite element simulation follows the red, downward-buckled curve obtained from the semi-analytic model. At intermediate intensity (60 mW $cm^{-2}$) in Fig. 5B and E, the light-induced curvature creates a sufficiently strong bias to tip the system into the upward-buckled state (blue curve). At still higher intensity in Fig. 5C and F, the finite element simulation again shows snap through, even though the state buckled downwards, towards the light, is predicted to be once again stable in the phase boundary obtained from the semi-analytical model (Fig. 3D).

Beginning from an unilluminated, nematic state, high intensity light will induce snap through as the system passes through a partially isomerized state, as denoted by the blue triangles outside the phase boundary in Fig. 3D. Beginning from the nematic state, however, causes the finite element simulation to pass through a partially isomerized state that is unstable, inducing snap through (grey conformation). Beginning from uniform illumination and narrowing the aperture causes the regions at the edges to relax from an isomerized, isotropic state back to the nematic state, keeping the strip in the downward buckled state (green conformation). The resulting shape and deflection angle is plotted in Fig. 5C and F, respectively.

Notably some cases in Fig. 4 and 5 show a discrepancy between the predictions from the finite element simulations and the semi-analytical model The reason for these differences is discussed further below.

### D. Dynamic trajectory to snap-through state

For the strain values studied here, we find that while both upward and downward buckled states are symmetric about the vertical axis, the snap-through trajectory between these states is asymmetric. Tracking the coordinates of the buckling strip in the finite element simulations reveals that the middle of the strip translates to one side concurrently with the vertical motion. Furthermore, stability predictions from the semi-analytical model suggest that cases where only a specific section of the strip can undergo isomerization will yield different behavior than cases where the isomerized regions can shift and grow with time. In particular, such cases, where the phase-change is confined to regions in the material frame by patterning during fabrication, (as in dual-phase nematic elastomers),[18] do not display the same snap-through behavior exhibited by the cases in the preceding results where isomerization was localized in the lab frame by an aperture.

We test this hypothesis *via* finite element simulations and confirm that cases where isomerized regions can grow and shift produce snap-through, whereas restricting the isomerization to specific elements traps the system in its initial state. Fig. 6A and B show the final states of these two different realizations for an initial strain of 0.3, intensity 60 mW $cm^{-2}$, and active region of width 200 μm determined by aperture width or material properties. These results reveal that an essential part of the mechanical instability that leads to snap through is the dynamic change in the area of the phase transition; the strip shifts slightly, changing which regions are isomerized by light, and thus inducing further deformation.

 

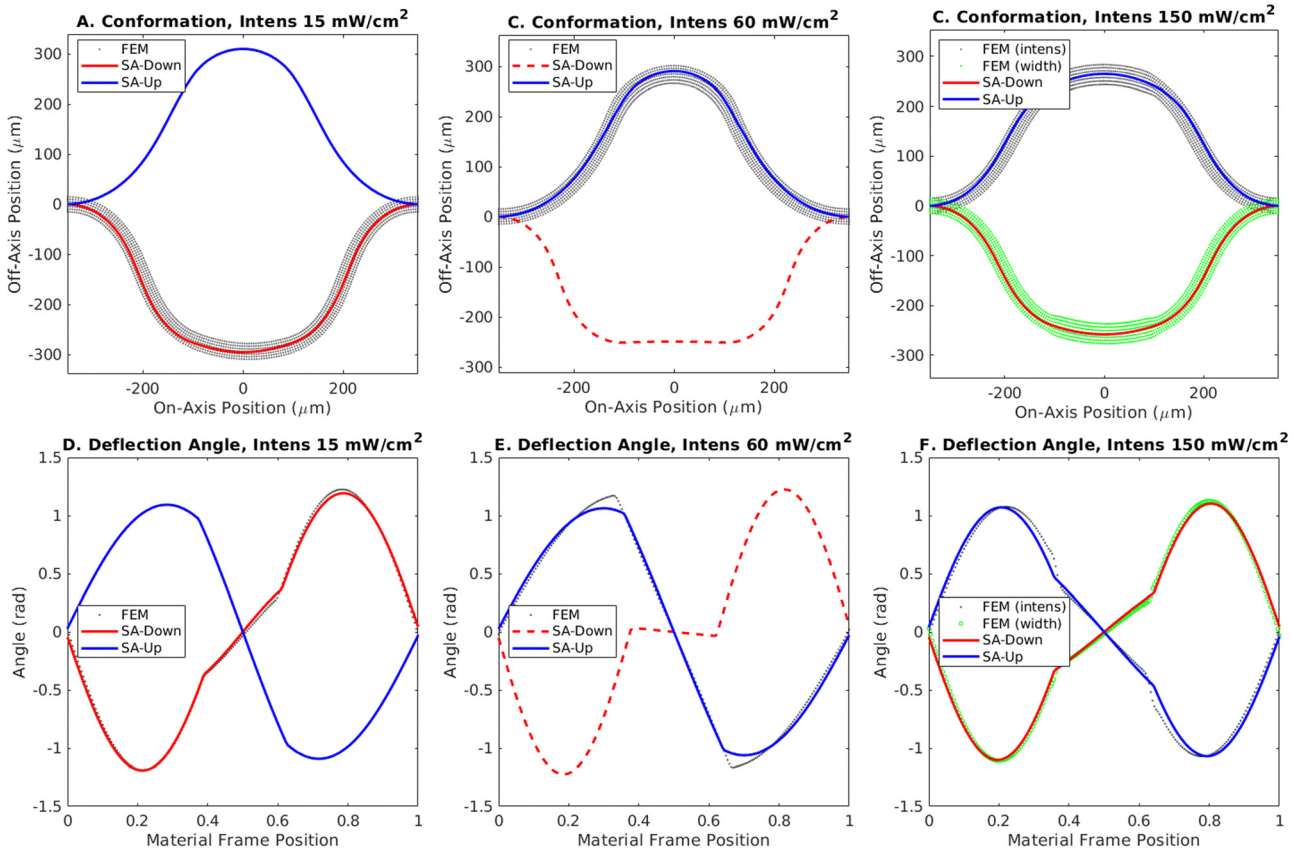


Fig. 5 Dependence of snap-through on light intensity for fixed aperture width (200 μm). Red and blue curves show the predicted shapes of the upward and downward buckled states, respectively, while black dotted shapes are the final conformations from finite element simulation. (A) At low intensity (15 mW cm$^{-2}$), the curvature induced by light is weak and the system remains in the downward-buckled state. (B) At medium intensity (60 mW cm$^{-2}$) the curvature induced by the light renders the downward buckled state unstable and it snaps through to the upward-buckled state. (C) At high intensity (150 mW cm$^{-2}$) both the downward buckled and upward buckled state are stable. Beginning from the nematic state, however, causes the finite element simulation to pass through a partially isomerized state that is unstable, inducing snap through (black dotted conformation). Beginning from uniform illumination and narrowing the aperture causes the regions at the edges to relax from an isomerized, isotropic state back to the nematic state, keeping the strip in the downward buckled state (green conformation). (D) Deflection angle for simulation in (A) alongside predictions from semi-analytical model. The discontinuity in the derivative, arising from the inhomogeneous light-induced curvature, is small at this intensity and the system remains stable in its initial state. (E) Deflection angle for simulation in (B). The larger induced curvature makes the upward-buckled state more energetically favorable relative to the downward buckled state. (F) Deflection angle for simulation in (C). The light-induced curvature decreases at high intensity, but the finite element simulation undergoes snap-through as it passes through a partially isomerized state. An alternate finite element simulation relaxed from an isotropic initial state demonstrates the stability of the downward-buckled state for these parameters (green conformation).

This result implies that the curvature and contraction induced by light must encompass time-dependent behavior to induce snap-through. In particular, Fig. 6C shows the trajectory of the finite element mesh node at the center of the strip as a function of time for the simulation producing Fig. 6A. The middle of the strip swings to one side in the horizontal direction, immediately prior to the rapid switching in the vertical position. The strip then settles back into a symmetric shape. Fig. 6D displays the isomerization as a function of time for the nodes on the surface of the mesh closest to the light. The illuminated region occupies the same width in the lab frame but shifts and grows in the material frame during the snap through.

After producing snap-through in one direction, the system can be reset without mechanical contact by altering the illuminated region *via* a photomask or screen. Making use of the fact that the curvature at the edges has the opposite sign of the curvature in the middle, we show that directing light at the edges of the strip can induce snap-through in a strip buckled away from the light, causing it to move towards the light. As shown in Fig. 7, this snap-through exhibits behavior similar to that for the case of photophobic snapping induced by centered light in Fig. 3–5. The black bars in Fig. 7A and B represent a screen which blocks the light from hitting the central region of the strip. Fig. 7A depicts the final states of the finite element simulation for a screen width of 400 μm at intensities of 15 mW cm$^{-2}$ and 90 mW cm$^{-2}$, under an initial strain of 0.3. At the lower intensity, the system remains buckled away from the light, but at the higher intensity, it snaps through towards the light. This demonstrates how increasing light above a certain threshold is necessary to overcome the energy barrier, analogous to Fig. 5.

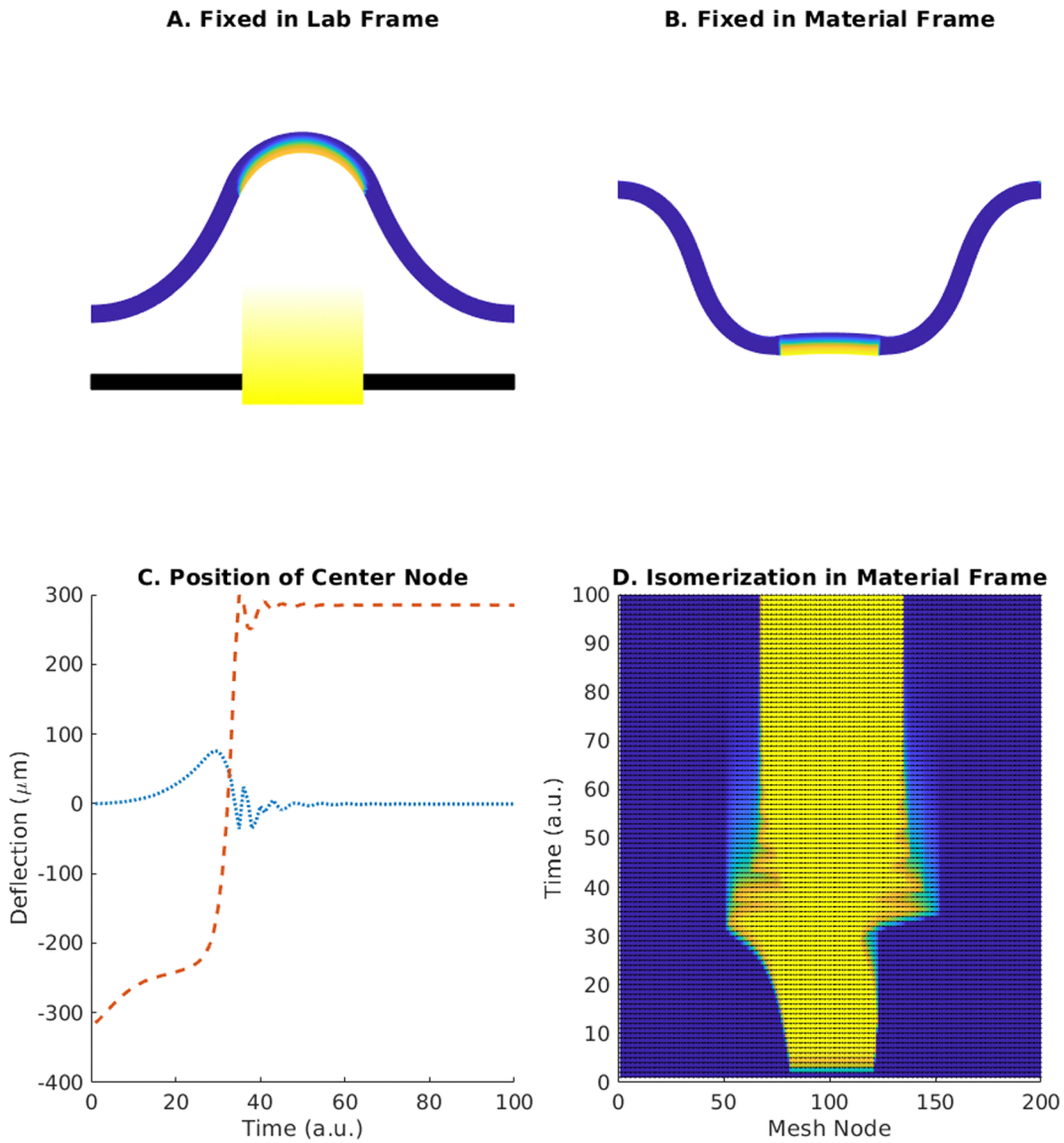


Fig. 6 Dependence of snap-through on time-dependent isomerization. (A) When the isomerized region is controlled by shining a light on a fixed region in the lab frame, the snap through phenomena described above can occur. The figure shows the final conformation from finite element simulation for an aperture width 200 μm and intensity 60 mW $cm^{-2}$. (B) When the isomerization is confined in the material frame, the system is trapped in the downward buckled state. The figure shows the final conformation from a finite element simulation at incident intensity 60 mW $cm^{-2}$ where isomerization is confined to the elements in a 200 μm region about the center in the pre-strain conformation. (C) Trajectory of center node of finite element mesh over time during snap-through. The horizontal position (blue dotted line) moves asymmetrically immediately prior to the vertical snap-through (orange dashed line). (D) Isomerization in the material frame over time. The horizontal motion in the previous panel causes a change in the regions of the material undergoing a phase change, altering where the material is deformed and curved. This degree of freedom is essential to snap-through for the boundary conditions studied here.

Fig. 7C shows the sensitivity of the snap-through phenomenon to the width of the screen blocking the central region from light. As with the aperture width in Fig. 4, this screen width must be neither too small nor too large. At a constant intensity of 30 mW $cm^{-2}$, initial strain 0.3, and a screen width of 500 μm, when only the edges are illuminated, the change is insufficient to induce snap-through. At 300 μm, the downward curvature induced by the light is enough to overcome the upward curvature at the edges and cause the system to transition. At 100 μm, most of the strip is illuminated and the competing interactions of the induced curvature with the varying curvature within the elastomer prevents it from snapping through.

The data collected from these simulations is plotted as a phase diagram in Fig. 7D (similar to Fig. 3D), illustrating the range of light intensity and screen width that can induce snap through in the opposite direction. The dashed line delineates the stable boundary predicted by our semi-analytical model. It should be noted that while snap-through away from the light can be triggered for pinned boundary conditions, where the

 

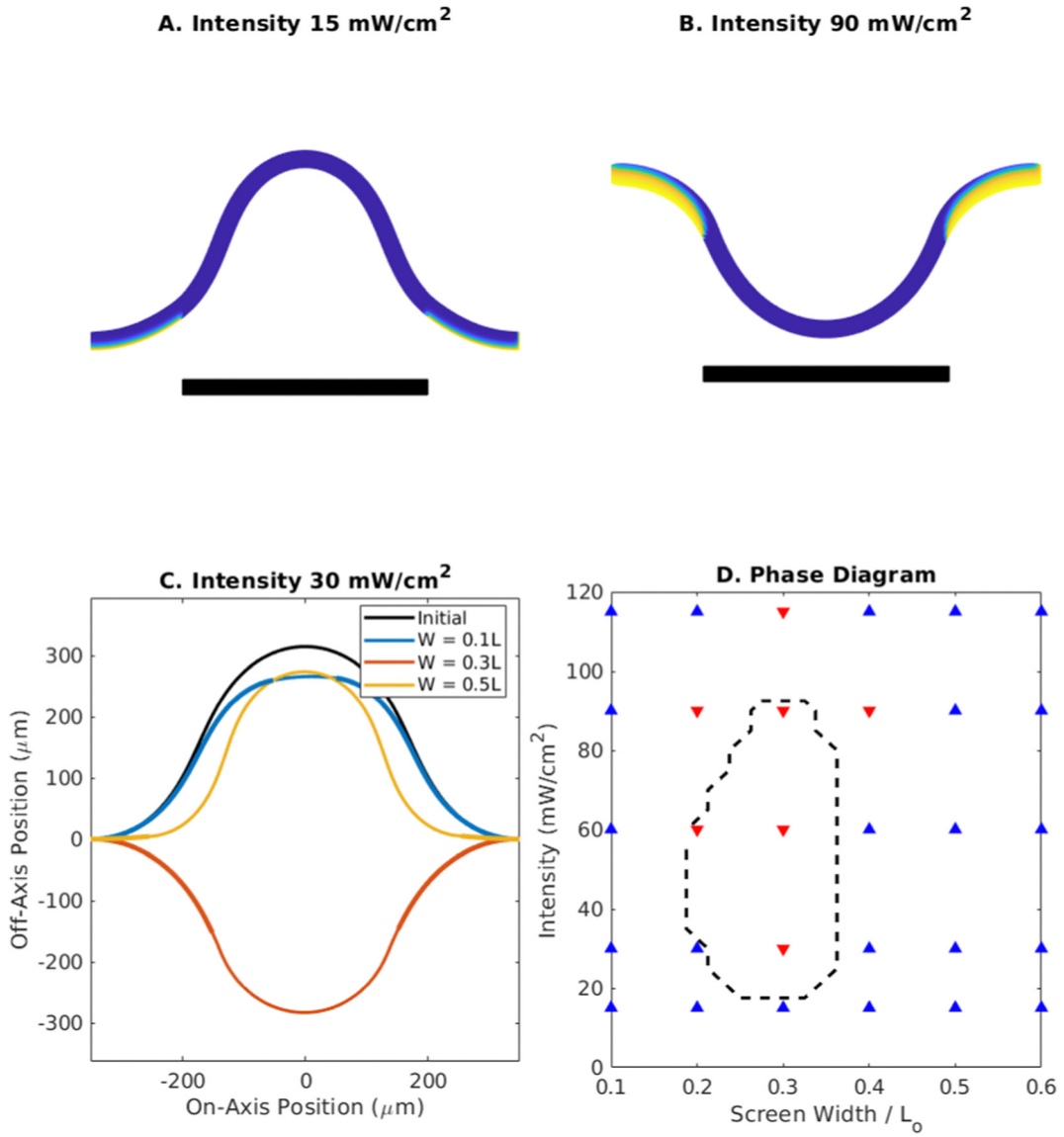


Fig. 7 Snap-through in opposite direction (A) final conformation from finite element simulation with intensity 15 mW cm$^{-2}$ and screen width 400 μm. The strip remains in the upward-buckled state. (B) Final conformation at higher intensity (90 mW cm$^{-2}$). The curvature induced by the bimorph at the edges causes the strip to snap through towards the light. (C) Effect of screen width variation at constant intensity 30 mW cm$^{-2}$. The initial conformation is indicated *via* the black line. For a narrow screen (100 μm, blue line), the energy difference between buckled states is insufficient to induce snap-through. For a wider screen (300 μm, orange line) the strip can reduce free energy by snapping through to the downward-buckled conformation. When a 500 μm region is blocked (yellow line) the system is stable in its original state. (D) Phase diagram showing the values of screen width and intensity for which finite element simulations initially buckled away from the light underwent snap-through towards the light (red) or remained in initial state (blue). Black dashed line indicates phase boundary predicted by semi-analytical model. As with the centered aperture, there is a range of intensities and widths bounded above and below for which snapthrough occurs.

angle at the ends of the strip is unconstrained, reversing the behavior in the manner described above requires the curvature of the strip to take on both positive and negative values along its length, which only occurs for the clamped boundary case.

### E. Buckling in initially flat strips

A number of fabrication schemes exist for LCE systems, which determine the orientation of the nematic director within the material *via* mechanical alignment,[19] shear flow,[20] surface alignment,[21] or direct ink writing.[22] Our model system involves the use of a magnetic field during cross-linking to align the director, decoupling this orientation from the spatial dimensions of the system.[12]

With the nematic director oriented orthogonal to the long axis of the strip, the strip will assume a flat geometry in the absence of light and increase in length under illumination (rather than contract as in Fig. 1). The increase in length for this geometry under illumination introduces strain when the ends are fixed, and can induce buckling in a thin clamped strip that is flat in the nematic state. Fig. 8 shows how length and

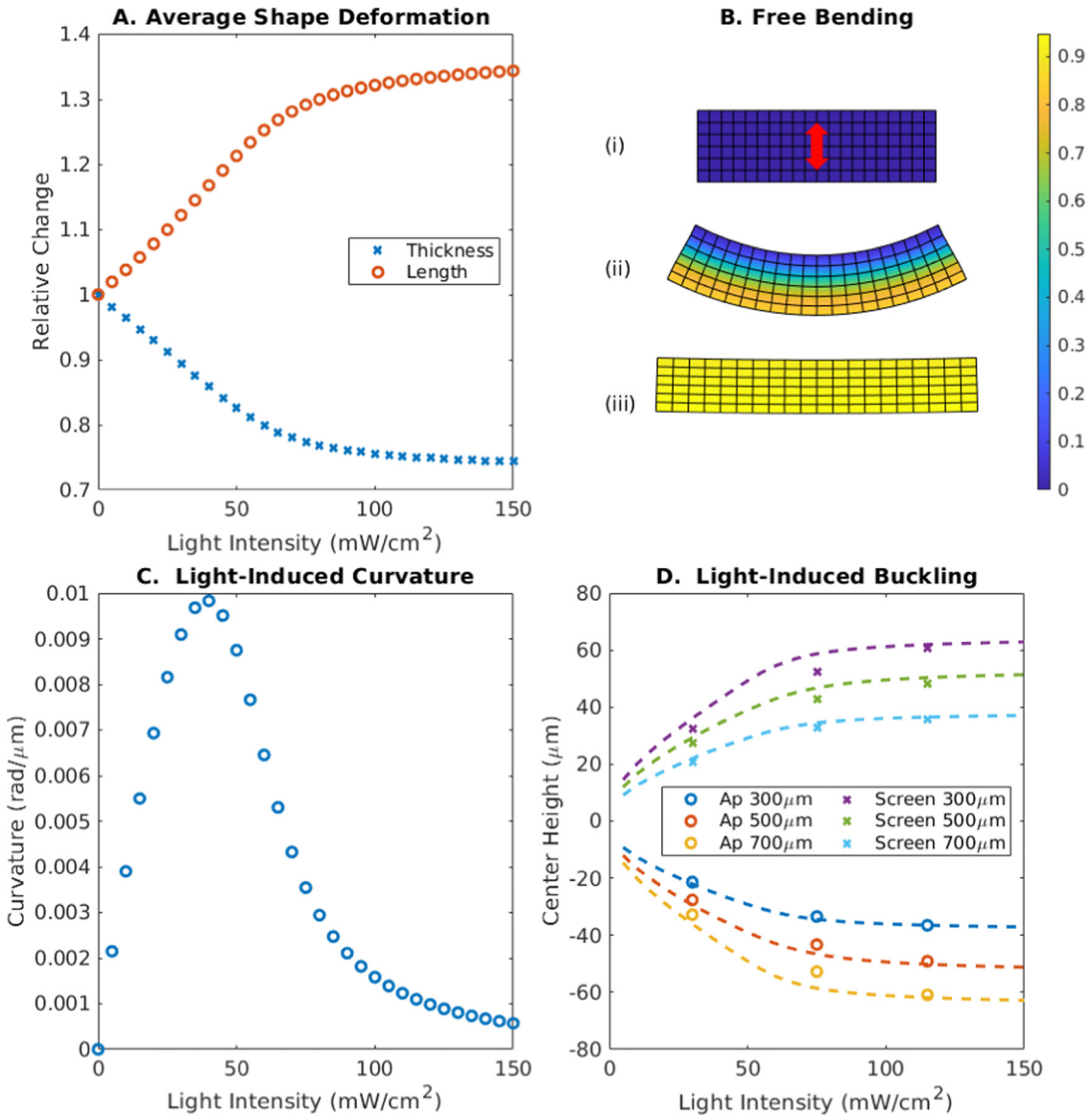


Fig. 8 Free LCE as a function of light intensity for orthogonal orientation of director. (A) Average length and height change through the thickness of the material *versus* intensity. Length increases by a factor of 1.34 at high intensity, with thickness decreasing by a factor 0.74. (B) Resulting conformations for zero intensity, intermediate intensity (45 mW cm$^{-2}$) and high intensity (150 mW cm$^{-2}$). Color indicates the degree of isomerization from 0 (blue) to 1 (yellow). At intermediate intensity, the expansion of the strip along the long axis and contraction along the thickness causes bending away from the light. At high intensity, this bending decreases. (C) Curvature induced in the LCE strip as a function of intensity. The induced curvature has the opposite sign *versus* Fig. 1D. The maximum value attained is 9.8 $\times$ 10$^{-3}$ rad μm$^{-1}$ at an intensity of 40 mW cm$^{-2}$. (D) Center deflection as a function of intensity for different illuminated areas at the center and edges. Circles and crosses represent finite element simulations for different aperture and screen widths, respectively, while dashed lines correspond to predictions from the semi-analytical model. In all cases, increasing the illuminated area and increasing the light intensity led to an increase in the amplitude of the deflection.

curvature vary for this geometry, in contrast to the director orientation along the strip in Fig. 1. In Fig. 8A, the length along the strip grows with respect to intensity. This reconfiguration is accompanied by the strip growing thinner, becoming easier to bend as it extends. The height contraction and length expansion reflect the rotation from Fig. 1B, with the length increasing by a factor 1.34$\times$ at high intensities and the height contracting by 0.74$\times$.

Furthermore, the induced curvature shown in Fig. 8B is away from the origin of the incident light, as the illuminated face increases in length by a greater amount than the opposite side of the material. This behavior reverses the sign of the induced curvature relative to that found in Fig. 1D, but displays similar qualitative behavior, first increasing then decreasing in magnitude as the isomerization front moves through the thickness of the material. The magnitude of this curvature is greater than that in Fig. 1, as the phase transition also makes the strip thinner and easier to bend as it progresses, achieving a maximum value of 9.8 $\times$ 10$^{-3}$ rad μm$^{-1}$ at an intensity of 40 mW cm$^{-2}$.

 

Fig. 8D shows the deflection of the center of the film as a function of light intensity, for different areas of illumination. The plot reveals the amplitude of the deflection increases monotonically with intensity, and with the area of illumination. The direction of the deflection is dictated by whether the center or the edges of the strip are illuminated: in the absence of an initial strain, center illumination will produce buckling downwards towards the light in this geometry (circles) while edge illumination will produce buckling upwards (crosses), away from the light. Removing the light will allow the strip to return to its initial flat state.

## IV. Conclusions

Snap-through of elastic systems under confinement enables the quick release of stored potential energy, permitting fast, large-amplitude actuation from the response of liquid crystalline elastomers. While this buckling can occur in different directions under physically symmetric conditions, either up or down, the direction can be controlled when the symmetry is broken by an external light source. This control can depend non-trivially on several different parameters, namely the intensity and position of the incident light. Both the curvature and contraction induced by the non-uniform phase transition dictate the energy difference between states and the barrier between these states. As the curvature of the buckled strip is non-uniform, the behavior is dependent upon where along the length any curvature change caused by light actually occurs.

Using two numerical methods in concert, we map a phase diagram predicting what range of intensities and beam widths can induce a transition between buckled states. By altering these parameters, snap-through in different directions can be achieved, allowing the system to be reset and triggered multiple times. Removing the light source will cause the system to settle into one of two stable states, storing information about the light stimulus.

When the director is oriented orthogonal to the long axis of the LCE strip, the nematic–isotropic transition will cause the strip to increase length, introducing additional strain rather than relieving it. This behavior can induce buckling in an initially flat strip. If the transition is localized *via* light, the direction of this buckling can be controlled by inducing curvature towards the light either at the ends or the center of the strip. Removing the light source will remove the buckling in this case, resetting the system for the formation of a new shape and allowing it to function as a rewriteable haptic interface.

## Author contributions

J. T. W. performed the simulations and analyzed the data. J. T. W. and A. C. B. conceived the project and wrote the manuscript. A. C. B. supervised the work.

## Conflicts of interest

There are no conflicts of interest to declare.

## Acknowledgements

A. C. B. gratefully acknowledges funding US Army Research Office under Award W911NF-17-1-0351 for efforts on developing the theoretical model and DOE under Award DE-SC0005247 for the development of the computational model. This research was supported in part by the University of Pittsburgh Center for Research Computing, RRID:SCR_022735, which is supported by NSF award number OAC-2117681.

## References

1 P. Rothemund, A. Ainla, L. Belding, D. J. Preston, S. Kurihara, Z. Suo and G. M. Whitesides, A Soft, Bistable Valve for Autonomous Control of Soft Actuators, *Sci. Robot.*, 2018, **3**(16), eaar7986, DOI: **10.1126/scirobotics.aar7986**.

2 W.-K. Lee, D. J. Preston, M. P. Nemitz, A. Nagarkar, A. K. MacKeith, B. Gorissen, N. Vasios, V. Sanchez, K. Bertoldi, L. Mahadevan and G. M. Whitesides, A Buckling-Sheet Ring Oscillator for Electronics-Free, Multimodal Locomotion, *Sci. Robot.*, 2022, **7**(63), eabg5812, DOI: **10.1126/scirobotics.abg5812**.

3 D. Yang, B. Mosadegh, A. Ainla, B. Lee, F. Khashai, Z. Suo, K. Bertoldi and G. M. Whitesides, Buckling of Elastomeric Beams Enables Actuation of Soft Machines, *Adv. Mater.*, 2015, **27**(41), 6323–6327, DOI: **10.1002/adma.201503188**.

4 D. S. Kim, Y.-J. Lee, Y. B. Kim, Y. Wang and S. Yang, Autonomous, Untethered Gait-like Synchronization of Lobed Loops Made from Liquid Crystal Elastomer Fibers via Spontaneous Snap-Through, *Sci. Adv.*, 2023, **9**(20), eadh5107, DOI: **10.1126/sciadv.adh5107**.

5 M. R. Shankar, M. L. Smith, V. P. Tondiglia, K. M. Lee, M. E. McConney, D. H. Wang, L.-S. Tan and T. J. White, Contactless, Photoinitiated Snap-through in Azobenzene-Functionalized Polymers, *Proc. Natl. Acad. Sci. U. S. A.*, 2013, **110**(47), 18792–18797, DOI: **10.1073/pnas.1313195110**.

6 K. Korner, A. S. Kuenstler, R. C. Hayward, B. Audoly and K. Bhattacharya, A Nonlinear Beam Model of Photomotile Structures, *Proc. Natl. Acad. Sci. U. S. A.*, 2020, **117**(18), 9762–9770, DOI: **10.1073/pnas.1915374117**.

7 D. Corbett, C. L. van Oosten and M. Warner, Nonlinear Dynamics of Optical Absorption of Intense Beams, *Phys. Rev. A: At., Mol., Opt. Phys.*, 2008, **78**(1), 013823, DOI: **10.1103/PhysRevA.78.013823**.

8 S. Li, M. M. Lerch, J. T. Waters, B. Deng, R. S. Martens, Y. Yao, D. Y. Kim, K. Bertoldi, A. Grinthal, A. C. Balazs and J. Aizenberg, Self-Regulated Non-Reciprocal Motions in Single-Material Microstructures, *Nature*, 2022, **605**(7908), 76–83, DOI: **10.1038/s41586-022-04561-z**.

9 J. T. Waters, S. Li, Y. Yao, M. M. Lerch, M. Aizenberg, J. Aizenberg and A. C. Balazs, Twist Again: Dynamically and Reversibly Controllable Chirality in Liquid Crystalline Elastomer Microposts, *Sci. Adv.*, 2020, **6**(13), eaay5349, DOI: **10.1126/sciadv.aay5349**.

10 R. V. Martinez, J. L. Branch, C. R. Fish, L. Jin, R. F. Shepherd, R. M. D. Nunes, Z. Suo and G. M. Whitesides, Robotic Tentacles with Three-Dimensional Mobility Based

on Flexible Elastomers, *Adv. Mater.*, 2013, **25**(2), 205–212, DOI: 10.1002/adma.201203002.

11 D. J. Preston, P. Rothemund, H. J. Jiang, M. P. Nemitz, J. Rawson, Z. Suo and G. M. Whitesides, Digital Logic for Soft Devices, *Proc. Natl. Acad. Sci. U. S. A.*, 2019, **116**(16), 7750–7759, DOI: 10.1073/pnas.1820672116.

12 Y. Yao, J. T. Waters, A. V. Shneidman, J. Cui, X. Wang, N. K. Mandsberg, S. Li, A. C. Balazs and J. Aizenberg, Multiresponsive Polymeric Microstructures with Encoded Predetermined and Self-Regulated Deformability, *Proc. Natl. Acad. Sci. U. S. A.*, 2018, **115**(51), 12950–12955, DOI: 10.1073/pnas.1811823115.

13 C. J. Camargo, H. Campanella, J. E. Marshall, N. Torras, K. Zinoviev, E. M. Terentjev and J. Esteve, Batch Fabrication of Optical Actuators Using Nanotube–Elastomer Composites towards Refreshable Braille Displays, *J. Micromech. Microeng.*, 2012, **22**(7), 075009, DOI: 10.1088/0960-1317/22/7/075009.

14 D. Liu, N. B. Tito and D. J. Broer, Protruding Organic Surfaces Triggered by In-Plane Electric Fields, *Nat. Commun.*, 2017, **8**(1), 1526, DOI: 10.1038/s41467-017-01448-w.

15 M. A. Meyers and K. K. Chawla, *Mechanical Behavior of Materials*, Cambridge University Press, 2008.

16 L. D. Landau, E. M. Lifshitz, A. M. Kosevich and L. P. Pitaevskii, *Theory of Elasticity*, Elsevier, 1986, vol. 7.

17 D. Corbett and M. Warner, Linear and Nonlinear Photo-induced Deformations of Cantilevers, *Phys. Rev. Lett.*, 2007, **99**(17), 174302, DOI: 10.1103/PhysRevLett.99.174302.

18 L. Liu, B. Geng, S. M. Sayed, B.-P. Lin, P. Keller, X.-Q. Zhang, Y. Sun and H. Yang, Single-Layer Dual-Phase Nematic Elastomer Films with Bending, Accordion-Folding, Curling and Buckling Motions, *Chem. Commun.*, 2017, **53**(11), 1844–1847, DOI: 10.1039/C6CC08976C.

19 J. Küpfer and H. Finkelmann, Nematic Liquid Single Crystal Elastomers, *Makromol. Chem., Rapid Commun.*, 1991, **12**(12), 717–726, DOI: 10.1002/marc.1991.030121211.

20 C. Ohm, M. Morys, F. R. Forst, L. Braun, A. Eremin, C. Serra, R. Stannarius and R. Zentel, Preparation of Actuating Fibres of Oriented Main-Chain Liquid Crystalline Elastomers by a Wetspinning Process, *Soft Matter*, 2011, **7**(8), 3730, DOI: 10.1039/c1sm05111c.

21 Y. Sawa, K. Urayama, T. Takigawa, A. DeSimone and L. Teresi, Thermally Driven Giant Bending of Liquid Crystal Elastomer Films with Hybrid Alignment, *Macromolecules*, 2010, **43**(9), 4362–4369, DOI: 10.1021/ma1003979.

22 A. Kotikian, R. L. Truby, J. W. Boley, T. J. White and J. A. Lewis, 3D Printing of Liquid Crystal Elastomeric Actuators with Spatially Programed Nematic Order, *Adv. Mater.*, 2018, **30**(10), 1706164, DOI: 10.1002/adma.201706164.

 